Cartesian Impedance Control of a UAV with a Robotic Arm

Vincenzo Lippiello and Fabio Ruggiero

PRISMA Lab, Dipartimento di Informatica e Sistemistica, Università degli Studi di Napoli Federico II, via Claudio 21, 80125, Naples, Italy (e-mail: vincenzo.lippiello@unina.it, fabio.ruggiero@unina.it).

Abstract: The dynamic model of a UAV with an attached robotic arm is derived in a symbolic matrix form through the Euler-Lagrangian formalism. A Cartesian impedance control, which provides a dynamic relationship between external generalized forces acting on the structure and the system motion, is then designed. The hovering control of a quadrotor, equipped with a 3-DOF robotic arm and subject to contact forces and external disturbances, is tested in a simulated case study.

Keywords: Mobile robots and vehicles. Space. Force and compliance control.

1. INTRODUCTION

Recently, the research community interest towards the field of aerial robotics is grown. As underlined by Grzonka et al. (2012), unmanned aerial vehicles (UAVs) are often employed in several "passive" applications, mainly in indoor scenarios, such as inspection, remote sensing, surveillance. Lately, these vehicles are used in "active" tasks such as grasping and manipulation.

Pounds et al. (2011) underline that the grasp of an object by a flying UAV arises several problems due to both the unstable dynamics of the vehicle and the coupling effects given by the presence of the object. Hence, Ghadiok et al. (2011) and Mellinger et al. (2011) properly design the gripper since it is a key feature in aerial grasping process.

The bigger the carried payload, the bigger should be the capacity of the single employed UAV. Maza et al. (2010) use multiple collaborative UAVs in order to perform a transportation task. Michael et al. (2011) address the static equilibrium problem of a grasped payload at a desired pose, as well as the consequent stability analysis.

However, the complete switching from "passive" tasks into "active" tasks requires mechanical structures in order to perform more complex actions. Mobile ground platforms (Yamamoto and Yun (1994); Korpela et al. (2012)), underwater vehicles (Antonelli (2006)) and space robots (Yoshida and Wilcox (2008)) can be taken as examples of this scenario. Therefore, UAVs equipped with a robotic arm could be an efficient solution providing an aerial vehicle with the capability of performing dexterous manipulation tasks, but this is not a widely adopted solution.

As well as the presence of a carried object creates coupling effects in the dynamic model of the system, in the same way a mounted robot arm provides even more issues since its dynamics depends on the actual configuration of the whole state of the system. Cheviron et al. (2009) and Nonami et al. (2010) provide the dynamic models of different UAVs structures, while Castillo et al. (2005) and Nonami et al. (2010) describe stabilization and tracking controls, respectively. Several other control strategies based on backstepping (Madani and Benallegue (2007); Bouabdallah and Siegwart (2007)), PD^2 and Coriolis and gyroscopic terms compensation (Tayebi and McGilvray (2006)), visual data (Altug et al. (2002)), port Hamiltonian framework (Mahony et al. (2011)) and so on, can be found in the literature. Nonami et al. (2010), as well as Mahony and Hamel (2004), assume that the orientation dynamics of the UAV are compensated with separated high-gain control loop, and thus they consider a hierarchical control for which a time scale separation exists between the translational dynamics (slow time scale) and the orientation (fast time scale). On the other hand, Siciliano et al. (2009) describe the dynamic model and control for classical robot manipulators.

In this paper, the dynamic model of the UAV plus robot arm system is introduced in a symbolic matrix form through the Euler-Lagrangian formalism. The high complexity and coupling between the terms could not allow the separation between translation and orientation dynamics. A Cartesian impedance control, described by Ott (2008), is here revisited in order to realize a desired dynamical relationship between the whole system motion and external generalized forces acting on the structure. This relationship is specified in terms of coordinates which describe the motion of the desired variables in the Cartesian space. The hovering control of a quadrotor, equipped with a 3-DOF robot arm and subject to contact forces and external disturbances acting on some points of the whole structure, is illustrated with a simulation case study.
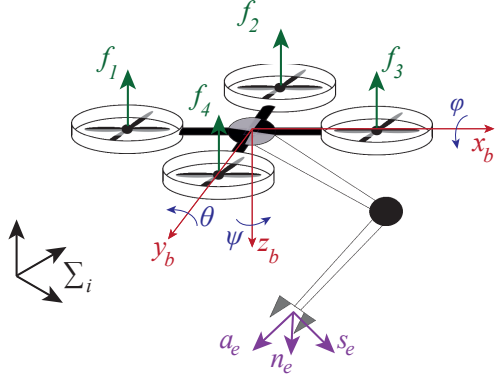
Fig. 1. UAV/Arm system illustration with the corresponding reference frames.

2. MODELING

2.1 Kinematic model

With reference to the system depicted in Fig. 1, let Σ_i be the world-fixed inertial reference frame and let Σ_b be the body-fixed reference frame placed at the vehicle center of mass. The absolute position of the UAV, i.e. of Σ_b, with respect to Σ_i is denoted by $\boldsymbol{p}_b = [x\ y\ z]^T$, while the UAV attitude is described by the yaw-pitch-roll Euler Angles $\boldsymbol{\phi}_b = [\psi\ \theta\ \varphi]^T$. Moreover, let $\dot{\boldsymbol{p}}_b$ denote the absolute linear velocity of the aerial vehicle, while $\dot{\boldsymbol{p}}_b^b$ describes the absolute linear velocity of the UAV with respect to Σ_b. On the other hand, let $\boldsymbol{\omega}_b$ be the absolute rotational velocity of the aerial vehicle, while $\boldsymbol{\omega}_b^b$ denotes the absolute rotational velocity of the UAV with respect to Σ_b. By denoting with $\dot{\boldsymbol{\phi}}_b$ the time derivative of $\boldsymbol{\phi}_b$, the following equations hold

$$\dot{\boldsymbol{p}}_b = \boldsymbol{R}_b \dot{\boldsymbol{p}}_b^b, \tag{1a}$$

$$\boldsymbol{\omega}_b = \boldsymbol{T}_b \dot{\boldsymbol{\phi}}_b, \tag{1b}$$

$$\boldsymbol{\omega}_b^b = \boldsymbol{R}_b^T \boldsymbol{\omega}_b = \boldsymbol{R}_b^T \boldsymbol{T}_b \dot{\boldsymbol{\phi}}_b = \boldsymbol{Q} \dot{\boldsymbol{\phi}}_b, \tag{1c}$$

where $\boldsymbol{R}_b \in \mathrm{SO}(3)$ is the rotation matrix denoting the orientation of Σ_b with respect to Σ_i, $\boldsymbol{T}_b$ is the (3×3) transformation matrix between the time derivative of $\boldsymbol{\phi}$ and the correspondent $\boldsymbol{\omega}_b$, and $\boldsymbol{Q} = \boldsymbol{R}_b^T \boldsymbol{T}_b$ maps the time derivative of $\boldsymbol{\phi}_b$ into the UAV angular velocity expressed with respect to Σ_b. Notice that Siciliano et al. (2009) affirm that the above matrices suffer from the so-called *representation singularities*, that is $\theta \neq \pm k\frac{\pi}{2}$, with $k = 1, 3, 5, \ldots$.

The direct kinematics of the UAV can be expressed in a compact form by the following matrix

$$\boldsymbol{A}_b(\boldsymbol{p}_b, \boldsymbol{\phi}_b) = \begin{bmatrix} \boldsymbol{R}_b & \boldsymbol{p}_b \\ \boldsymbol{0}^T & 1 \end{bmatrix}. \tag{2}$$

In the considered system, a robotic manipulator is attached to the UAV. Notice that the following derivation about the kinematic and dynamic models of the system does not depend on the particular choice of where the manipulator is attached. Depending on the specific configuration, e.g. quadrotor, ducted-fun, and so on, the best mounting of the manipulator in order to have a self-stabilizing behavior will be considered (see Fig. 2). The arm consists of n rigid links connected by means of joints q_i, with $i = 1, \ldots, n$. The end of the kinematic chain, that

Fig. 2. Examples of UAVs endowed with a manipulator: on the left the ARCAS-project concept; on the right the AIRobots-project prototype.

is not connected to the UAV basis, is an end-effector, e.g. a gripper. Hence, the direct kinematics function can be computed with respect to Σ_b, and it is expressed by

$$\boldsymbol{A}_e^b(\boldsymbol{q}) = \begin{bmatrix} \boldsymbol{n}_e^b(\boldsymbol{q}) & \boldsymbol{s}_e^b(\boldsymbol{q}) & \boldsymbol{a}_e^b(\boldsymbol{q}) & \boldsymbol{p}_e^b(\boldsymbol{q}) \\ 0 & 0 & 0 & 1 \end{bmatrix}, \tag{3}$$

where $\boldsymbol{q}$ is the $(n \times 1)$ vector of joint variables, $(\boldsymbol{n}_e^b, \boldsymbol{b}_e^b, \boldsymbol{a}_e^b)$ are the unit vectors of a frame attached to the end-effector, and $\boldsymbol{p}_e^b$ is the position vector of the origin of such a frame with respect to Σ_b. By combining (2) and (3), it is possible to obtain the absolute pose of the manipulator

$$\boldsymbol{A}_e(\boldsymbol{\xi}) = \boldsymbol{A}_b \boldsymbol{A}_e^b, \tag{4}$$

where $\boldsymbol{\xi} = \begin{bmatrix} \boldsymbol{p}_b^T & \boldsymbol{\phi}_b^T & q_1 & \ldots & q_n \end{bmatrix}^T$ is the generalized joint vector of $n_\xi = 6 + n$ components.

If the orientation of the manipulator is expressed in terms of a minimal representation $\boldsymbol{\phi}_e$, the direct kinematics equation can be also written in the following form $\boldsymbol{x} = \boldsymbol{k}(\boldsymbol{\xi})$, where $\boldsymbol{k}(\cdot)$ is an $(m \times 1)$ vector function, nonlinear in general, and $\boldsymbol{x}$ is an $(m \times 1)$ vector describing the system configuration through a minimal representation of the orientation. The linear mapping between the time derivative of $\boldsymbol{x}$ and $\dot{\boldsymbol{\xi}}$ is given by

$$\dot{\boldsymbol{x}} = \boldsymbol{J} \dot{\boldsymbol{\xi}}, \tag{5}$$

where the $(m \times n_\xi)$ matrix $\boldsymbol{J}$ is the so-called Jacobian of the system, derived via differentiation of $\boldsymbol{k}(\cdot)$.

Since in the following subsection the whole system dynamics will be derived, it is useful to introduce a frame for each link of the manipulator. The origin of each of these frames is placed at the link's center of mass, while the axes are coincident with the inertia central axes. By denoting with $\boldsymbol{p}_{l_i}$ the position of the center of mass of the link i with respect to Σ_i, the following relationship holds

$$\boldsymbol{p}_{l_i} = \boldsymbol{p}_b + \boldsymbol{R}_b \boldsymbol{p}_{bl_i}^b, \tag{6}$$

where $\boldsymbol{p}_{bl_i}^b$ denotes the vector position of the center of mass of the link i with respect to Σ_b. Moreover, Siciliano et al. (2009) consider the following expressions

$$\dot{\boldsymbol{p}}_{bl_i}^b = \boldsymbol{J}_{P1}^{(l_i)} \dot{q}_1 + \ldots + \boldsymbol{J}_{Pi}^{(l_i)} \dot{q}_i = \boldsymbol{J}_P^{(l_i)} \dot{\boldsymbol{q}} \tag{7a}$$

$$\boldsymbol{\omega}_{l_i}^b = \boldsymbol{J}_{O1}^{(l_i)} \dot{q}_1 + \ldots + \boldsymbol{J}_{Oi}^{(l_i)} \dot{q}_i = \boldsymbol{J}_O^{(l_i)} \dot{\boldsymbol{q}}, \tag{7b}$$

where $\boldsymbol{\omega}_{l_i}^b$ is the angular velocity of the i-th manipulator frame with respect to Σ_b, and where $\boldsymbol{J}_P^{(l_i)}$ and $\boldsymbol{J}_O^{(l_i)}$ are the contributions of the Jacobian columns relative to the joint velocities up to the current link i.

Deriving (6) with respect to time and taking into account (7) yield

$$\dot{\boldsymbol{p}}_{l_i} = \dot{\boldsymbol{p}}_b - \boldsymbol{S}(\boldsymbol{R}_b \boldsymbol{p}_{bl_i}^b)\boldsymbol{\omega}_b + \boldsymbol{R}_b \boldsymbol{J}_P^{(l_i)} \dot{\boldsymbol{q}}, \tag{8}$$

where $\boldsymbol{S}(\cdot)$ denotes the skew-symmetric matrix, and in which the anti-commutative property of the cross product has been taken into account. A similar expression can be derived for the angular velocity

$$\boldsymbol{\omega}_{l_i} = \boldsymbol{\omega}_b + \boldsymbol{R}_b \boldsymbol{J}_O^{(l_i)} \dot{\boldsymbol{q}}. \tag{9}$$

2.2 Dynamic model

The dynamic model can be derived by considering the so-called *Euler-Lagrange formulation*, in which the mechanical structure can be characterized by the function $\mathcal{L} = \mathcal{K} - \mathcal{U}$, where $\mathcal{K}$ and $\mathcal{U}$ denote the total kinetic and potential energies of the system, respectively. The Lagrange equations are then expressed by

$$\frac{d}{dt} \frac{\partial \mathcal{L}}{\partial \dot{\xi}_i} - \frac{\partial \mathcal{L}}{\partial \xi_i} = u_i, \tag{10}$$

where $i = 1, \ldots, n_\xi$, ξ_i is the i-th generalized coordinate of $\boldsymbol{\xi}$, and u_i is the associated i-th generalized force.

The total kinetic energy is given by the sum of the contributions relative to the motion of the aerial vehicle and the motion of each link of the manipulator

$$\mathcal{K} = \mathcal{K}_b + \sum_{i=1}^n \mathcal{K}_{l_i}, \tag{11}$$

where $\mathcal{K}_b$ is the kinetic energy associated to the UAV, while $\mathcal{K}_{l_i}$ is the kinetic energy of the link i.

The UAV kinetic energy contribution is given by

$$\mathcal{K}_b = \frac{1}{2} m_b \dot{\boldsymbol{p}}_p^{\mathrm{T}} \dot{\boldsymbol{p}}_p + \frac{1}{2} \boldsymbol{\omega}_b^{\mathrm{T}} \boldsymbol{R}_b \boldsymbol{H}_b \boldsymbol{R}_b^{\mathrm{T}} \boldsymbol{\omega}_b,$$

where m_b and $\boldsymbol{H}_b$ are respectively the mass and the inertia matrix of the UAV. Notice that $\boldsymbol{H}_b$ is constant since it is expressed with respect to Σ_b. By taking into account (1c), the previous contribution can be rewritten as follows

$$\mathcal{K}_b = \frac{1}{2} m_b \dot{\boldsymbol{p}}_p^{\mathrm{T}} \dot{\boldsymbol{p}}_p + \frac{1}{2} \dot{\boldsymbol{\phi}}_b^{\mathrm{T}} \boldsymbol{Q}^{\mathrm{T}} \boldsymbol{H}_b \boldsymbol{Q} \dot{\boldsymbol{\phi}}_b. \tag{12}$$

On the other hand, the kinetic energy contribution of each link of the robotic manipulator is given by

$$\mathcal{K}_{l_i} = \frac{1}{2} m_{l_i} \dot{\boldsymbol{p}}_{l_i}^{\mathrm{T}} \dot{\boldsymbol{p}}_{l_i} + \frac{1}{2} \boldsymbol{\omega}_{l_i}^{\mathrm{T}} \boldsymbol{R}_b \boldsymbol{R}_{l_i}^b \boldsymbol{H}_{l_i} \boldsymbol{R}_b^{l_i} \boldsymbol{R}_b^{\mathrm{T}} \boldsymbol{\omega}_{l_i}, \tag{13}$$

where $\boldsymbol{R}_{l_i}^b$ is the rotation matrix between the frame associated to the center of mass of the i-th link and Σ_b, while m_{l_i} and $\boldsymbol{H}_{l_i}$ are the mass and the constant inertia matrix of the same link i, respectively.

By taking into account (1c), (8), (9), (12) and (13), the total kinetic energy (11) can be expressed as

$$\mathcal{K} = \frac{1}{2} \dot{\boldsymbol{\xi}}^{\mathrm{T}} \boldsymbol{B} \dot{\boldsymbol{\xi}}, \tag{14}$$

where $\boldsymbol{B}$ is an $(n_\xi \times n_\xi)$ symmetric and positive definite inertia matrix, whose block-elements are

$$\boldsymbol{B}_{11} = \left(m_b + \sum_{i=1}^n m_{l_i} \right) \boldsymbol{I}_3$$

$$\boldsymbol{B}_{22} = \boldsymbol{Q}^{\mathrm{T}} \boldsymbol{H}_b \boldsymbol{Q} + \sum_{i=1}^n \left(m_{l_i} \boldsymbol{T}_b^{\mathrm{T}} \boldsymbol{S}(\boldsymbol{R}_b \boldsymbol{p}_{bl_i}^b)^{\mathrm{T}} \boldsymbol{S}(\boldsymbol{R}_b \boldsymbol{p}_{bl_i}^b) \boldsymbol{T}_b \right.$$
$$\left. + \boldsymbol{Q}^{\mathrm{T}} \boldsymbol{R}_{l_i}^b \boldsymbol{H}_{l_i} \boldsymbol{R}_b^{l_i} \boldsymbol{Q} \right)$$

$$\boldsymbol{B}_{33} = \sum_{i=1}^n \left(m_{l_i} \boldsymbol{J}_P^{(l_i)\mathrm{T}} \boldsymbol{J}_P^{(l_i)} + \boldsymbol{J}_O^{(l_i)\mathrm{T}} \boldsymbol{R}_{l_i}^b \boldsymbol{H}_{l_i} \boldsymbol{R}_b^{l_i} \boldsymbol{J}_O^{(l_i)} \right)$$

$$\boldsymbol{B}_{12} = \boldsymbol{B}_{21}^{\mathrm{T}} = -\sum_{i=1}^n \left(m_{l_i} \boldsymbol{S}(\boldsymbol{R}_b \boldsymbol{p}_{bl_i}^b) \boldsymbol{T}_b \right)$$

$$\boldsymbol{B}_{13} = \boldsymbol{B}_{31}^{\mathrm{T}} = \sum_{i=1}^n \left(m_{l_i} \boldsymbol{R}_b \boldsymbol{J}_P^{(l_i)} \right)$$

$$\boldsymbol{B}_{23} = \boldsymbol{B}_{32}^{\mathrm{T}} = \sum_{i=1}^n \left(\boldsymbol{Q}^{\mathrm{T}} \boldsymbol{R}_{l_i}^b \boldsymbol{H}_{l_i} \boldsymbol{R}_b^{l_i} \boldsymbol{J}_O^{(l_i)} \right.$$
$$\left. - m_{l_i} \boldsymbol{T}_b^{\mathrm{T}} \boldsymbol{S}(\boldsymbol{R}_b \boldsymbol{p}_{bl_i}^b)^{\mathrm{T}} \boldsymbol{R}_b \boldsymbol{J}_P^{(l_i)} \right),$$

in which $\boldsymbol{I}_\alpha$ denotes the $(\alpha \times \alpha)$ identity matrix.

The potential energy stored in the system is given by the sum of the contribution relative to the vehicle and the contribution relative to each manipulator link

$$\mathcal{U} = \mathcal{U}_b + \sum_{i=1}^n \mathcal{U}_{l_i}, \tag{15}$$

where $\mathcal{U}_b$ is the potential energy associated to the UAV, while $\mathcal{U}_{l_i}$ is the potential energy of the link i.

The UAV potential energy is thus given by

$$\mathcal{U}_b = m_b g \boldsymbol{e}_3^{\mathrm{T}} \boldsymbol{p}_b, \tag{16}$$

where $g = 9.8$ m/s^2 is the gravity acceleration value and $\boldsymbol{e}_3$ is a (3×1) vector selecting the axes of Σ_i where the gravity acts, i.e. $\boldsymbol{e}_3 = [0\ 0\ 1]^{\mathrm{T}}$ if gravity acts along the z axis of Σ_i.

On the other hand, by taking into account (6), the potential energy contribution of each link of the robotic manipulator is given by

$$\mathcal{U}_{l_i} = m_{l_i} g \boldsymbol{e}_3^{\mathrm{T}} \left(\boldsymbol{p}_b + \boldsymbol{R}_b \boldsymbol{p}_{bl_i}^b \right). \tag{17}$$

Thereby, by taking into account (16) and (17), the potential energy of the system (15) can be written as

$$\mathcal{U} = m_b g \boldsymbol{e}_3^{\mathrm{T}} \boldsymbol{p}_b + g \sum_{i=1}^n \left[m_{l_i} \boldsymbol{e}_3^{\mathrm{T}} \left(\boldsymbol{p}_b + \boldsymbol{R}_b \boldsymbol{p}_{bl_i}^b \right) \right]. \tag{18}$$

Then, having computed the total kinetic and potential energies of the system in (14) and (18), by computing the Lagrange equations (10) and by considering the *Christoffel symbols of the first type* (Siciliano et al. (2009)), the dynamics of the whole UAV and robotic arm system can be written as

$$\boldsymbol{B}(\boldsymbol{\xi}) \ddot{\boldsymbol{\xi}} + \boldsymbol{C}(\boldsymbol{\xi}, \dot{\boldsymbol{\xi}}) \dot{\boldsymbol{\xi}} + \boldsymbol{g}(\boldsymbol{\xi}) = \boldsymbol{u} + \boldsymbol{u}_{ext}, \tag{19}$$

in which the $(n_\xi \times 1)$ vector $\boldsymbol{u}$ represents the generalized input forces, $\boldsymbol{g}(\boldsymbol{\xi}) = (\partial \mathcal{U}(\boldsymbol{\xi})/\partial \boldsymbol{\xi})^\mathrm{T}$ and $\boldsymbol{C}$ is a suitable $(n_\xi \times n_\xi)$ matrix whose generic element is

$$c_{ij} = \sum_{k=1}^{n_\xi} \frac{1}{2}\left(\frac{\partial b_{ij}}{\partial \xi_k} + \frac{\partial b_{ik}}{\partial \xi_j} + \frac{\partial b_{jk}}{\partial \xi_i}\right)\dot{\xi}_k,$$

where b_{ij} is the generic element of $\boldsymbol{B}(\boldsymbol{\xi})$, with $i, j = 1, \ldots, n_\xi$. The last term $\boldsymbol{u}_{ext}$ in (19) shapes the effects of external generalized forces at the joint level.

In the quadrotor case of Fig. 1, by supposing negligible the aerodynamic effects and by supposing low-speed displacements, the vector $\boldsymbol{u}$ has the following expression

$$\boldsymbol{u} = \bar{\boldsymbol{R}}_b \boldsymbol{N} \boldsymbol{f} = \boldsymbol{\Xi} \boldsymbol{f}, \qquad (20)$$

where $\boldsymbol{f} = \begin{bmatrix} \boldsymbol{f}^\mathrm{T} & \boldsymbol{\tau}^\mathrm{T} \end{bmatrix}^\mathrm{T}$, with $\boldsymbol{f}$ the (4×1) input vector of forces given by the quadrotor motors and $\boldsymbol{\tau}$ the $(n \times 1)$ input vector of the manipulator actuation torques. Moreover, $\bar{\boldsymbol{R}}_b = \mathrm{diag}(\boldsymbol{R}_b, \boldsymbol{Q}^\mathrm{T}, \boldsymbol{I}_n)$ is an $(n_\xi \times n_\xi)$ matrix, and $\boldsymbol{N} = \mathrm{diag}(\boldsymbol{\Omega}, \boldsymbol{I}_n)$ is an $(n_\xi \times 4 + n)$ matrix, in which

$$\boldsymbol{\Omega} = \begin{bmatrix} 0 & 0 & 0 & 0 \\ 0 & 0 & 0 & 0 \\ 1 & 1 & 1 & 1 \\ 0 & d & 0 & -d \\ -d & 0 & d & 0 \\ c & -c & c & -c \end{bmatrix},$$

where d is the distance from a motor to the center of the vehicle and $c > 0$ is the drag factor.

3. CARTESIAN IMPEDANCE CONTROL

Impedance control is still a rather far adopted solution in aerial robotics applications, while, on the other hand, it is often employed in robot manipulation tasks. In this paper, the goal of impedance control is to realize a particular desired dynamical relationship between the UAV and robotic arm motion and the external forces. Usually, as done by Siciliano and Villani (1999), classical impedance controllers require the measurements of the external forces, which typically act on the manipulator end-effector. This situation is unfeasible in aerial robotics applications since other disturbances and unmodelled aerodynamic effects can arise during the performed task. Hence, the method proposed by Ott (2008) can be revised in such a context.

Consider a vector of Cartesian coordinates $\boldsymbol{x}$ with $m = n_\xi$. With this choice, the Jacobian $\boldsymbol{J}$ has $(n_\xi \times n_\xi)$ dimensions. Deriving (5) with respect to time yields

$$\ddot{\boldsymbol{x}} = \boldsymbol{J}\ddot{\boldsymbol{\xi}} + \dot{\boldsymbol{J}}\dot{\boldsymbol{\xi}}. \qquad (21)$$

Let $\boldsymbol{x}_d$, $\dot{\boldsymbol{x}}_d$ and $\ddot{\boldsymbol{x}}_d$ be the desired, even time-varying, desired *virtual* position, velocity and acceleration, respectively. The word virtual is used since this desired configuration will be reached only along the unconstrained motion directions due to the presence of the external forces. By denoting with $\tilde{\boldsymbol{x}} = \boldsymbol{x}_d - \boldsymbol{x}$ the actual position error, the following control law can be defined

$$\boldsymbol{u} = \boldsymbol{g} + \boldsymbol{J}^\mathrm{T}\left(\boldsymbol{B}_x\ddot{\boldsymbol{x}}_d + \boldsymbol{C}_x\dot{\boldsymbol{x}}_d + \boldsymbol{K}_D\dot{\tilde{\boldsymbol{x}}} + \boldsymbol{K}_P\tilde{\boldsymbol{x}}\right), \qquad (22)$$

where $\boldsymbol{K}_P$ and $\boldsymbol{K}_D$ are $(n_\xi \times n_\xi)$ symmetric and positive definite matrices of desired stiffness and damping, respectively, while $\boldsymbol{B}_x$ and $\boldsymbol{C}_x$ are the inertia and Coriolis
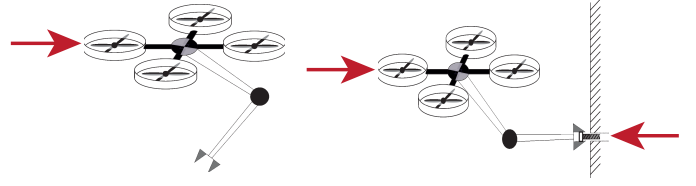

Fig. 3. On the left, a schematic representation of the simulated case study A. On the right, a schematic representation of the simulated case study B.

matrices, with respect to the $\boldsymbol{x}$, variables and defined as follows

$$\boldsymbol{B}_x = \boldsymbol{J}(\boldsymbol{\xi})^{-\mathrm{T}}\boldsymbol{B}(\boldsymbol{\xi})\boldsymbol{J}(\boldsymbol{\xi})^{-1}$$

$$\boldsymbol{C}_x = \boldsymbol{J}(\boldsymbol{\xi})^{-\mathrm{T}}\left(\boldsymbol{C}(\boldsymbol{\xi}, \dot{\boldsymbol{\xi}}) - \boldsymbol{B}(\boldsymbol{\xi})\boldsymbol{J}(\boldsymbol{\xi})^{-1}\dot{\boldsymbol{J}}(\boldsymbol{\xi})\right)\boldsymbol{J}(\boldsymbol{\xi})^{-1}.$$

By substituting (22) into (19), and by taking into account (5) and (21), the equations describing the closed-loop system behaviour, and hence the desired dynamic relationship, namely are

$$\boldsymbol{B}_x\ddot{\tilde{\boldsymbol{x}}} + (\boldsymbol{C}_x + \boldsymbol{K}_D)\dot{\tilde{\boldsymbol{x}}} + \boldsymbol{K}_P\tilde{\boldsymbol{x}} = \boldsymbol{f}_{ext}, \qquad (23)$$

where the $(n_\xi \times 1)$ vector $\boldsymbol{f}_{ext}$ shapes the effects of external generalized forces at the Cartesian coordinate level. A way to choose the stiffness and damping matrices $\boldsymbol{K}_P$ and $\boldsymbol{K}_D$ is illustrated by Ott (2008).

Even in the case of free-motion, $\boldsymbol{f}_{ext} = \boldsymbol{0}$, the stability analysis of the system (23) is not obvious since the matrix $\boldsymbol{B}_x$ is configuration dependent and time-varying. By considering the following time-varying candidate Lyapunov function

$$V = \frac{1}{2}\dot{\tilde{\boldsymbol{x}}}^\mathrm{T}\boldsymbol{B}_x\dot{\tilde{\boldsymbol{x}}} + \frac{1}{2}\tilde{\boldsymbol{x}}^\mathrm{T}\boldsymbol{K}_P\tilde{\boldsymbol{x}},$$

and by taking into account (19) and (22), it is possible to show that $\dot{V}$ is negative semi-definite. Hence, only stability can be ensured. However, by considering the Cartesian configuration space $\mathcal{C}$ in which the Jacobian $\boldsymbol{J}$ is always invertible, it is possible to show the asymptotic stability of the system (23). Moreover, if $\mathcal{C}$ corresponds to the entire state space $\mathcal{R}^{n_\xi}$, then Santibanez and Kelly (1997) show that (23) is uniformly globally asymptotically stable.

On the other hand, in case of constrained motion, $\boldsymbol{f}_{ext} \neq \boldsymbol{0}$, the above described stability can be reached only in the unconstrained Cartesian directions. Moreover, it is worth noticing that in case of regulation control problems, i.e. $\dot{\boldsymbol{x}}_d = \boldsymbol{0}$, the effort for computing (22) drastically reduces, and the system (23) becomes a passive mapping between $\boldsymbol{f}_{ext}$ and $\dot{\boldsymbol{x}}$.

4. SIMULATION RESULTS

The results of two simulated case studies, namely A and B, performed through the MATLAB/SIMULINK environment are presented in this section. With reference to Fig. 1, the dynamic model of an ASCTEC PELICAN quadrotor with mass $m_b = 2$ kg and inertia matrix $\boldsymbol{H}_b = \mathrm{diag}(1.24, 1.24, 2.48)$ m^{2}kg has been derived. A 3-DOF robotic arm mounted at the bottom of the quadrotor is considered. The robotic manipulator is composed of 2 links of 15 cm and 5 cm length, respectively, and 3 revolute joints; in particular, the first two axes intersect in a common point. The corresponding centers of mass are

(a) Case study A. Rigid behavior. Error norm of the manipulator end-effector position.

(b) Case study A. Rigid behavior. Error norm of the quadrotor position.

(c) Case study A. Rigid behavior. Error norm of the quadrotor orientation.

(d) Case study A. Compliant behavior. Error norm of the manipulator end-effector position.

(e) Case study A. Compliant behavior. Error norm of the quadrotor position.

(f) Case study A. Compliant behavior. Error norm of the quadrotor orientation.

(g) Case study B. Error norm of the manipulator end-effector position.

(h) Case study B. Error norm of the quadrotor position.

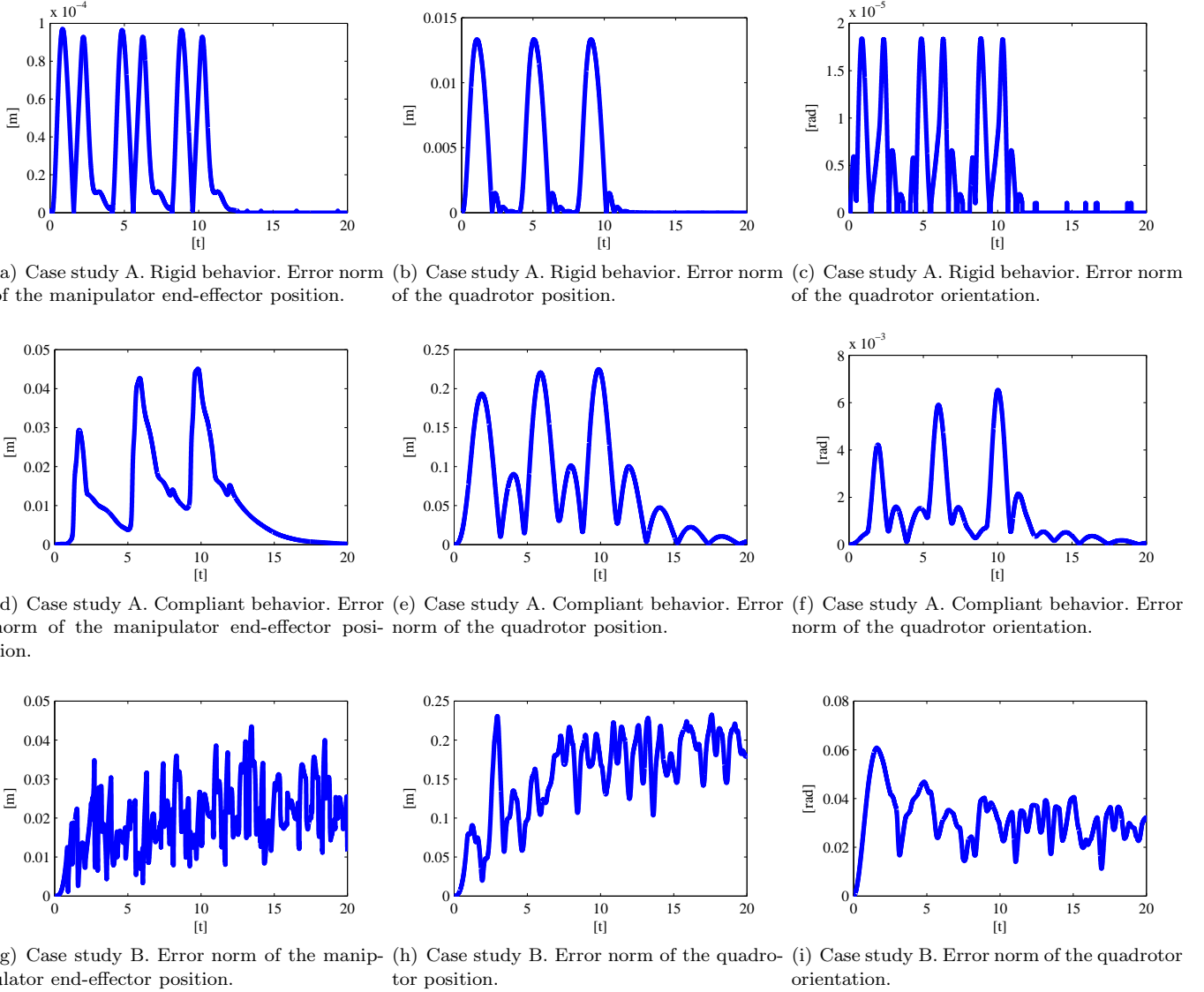(i) Case study B. Error norm of the quadrotor orientation.

Fig. 4. Time histories simulating the case studies A and B.

located at the middle of each link. The mass and the inertia around the rotational axis for the first link are 0.049 kg and 0.0011 m²kg, respectively, while for the second link are 0.05 kg and $1.25e^{-4}$ m²kg. These values have been retrieved by building such a manipulator into a 3D CAD environment. Finally, a distance of 0.1 m, along the vertical axis z_b of Σ_b, is present between the center of Σ_b and the spherical joint reference frame. Being $n = 3$, and thus $n_\xi = 9$, the chosen Cartesian variables for the control are the pose of the aerial vehicle and the position of the manipulator end-effector, that is $\boldsymbol{x} = \begin{bmatrix} \boldsymbol{p}_b^\mathrm{T} & \boldsymbol{\phi}_b^\mathrm{T} & \boldsymbol{p}_e^\mathrm{T} \end{bmatrix}^\mathrm{T}$, while the initial values of the system generalized joints are set to $\boldsymbol{\xi} = \begin{bmatrix} 0 & 0 & 2 & 0 & 0 & 0 & -\pi/2 & 0 & \pi/2 \end{bmatrix}^\mathrm{T}$.

The aim of case study A is to perform an hovering control action while an external force acts along the $\boldsymbol{x}_b$ axis of Σ_b, simulating, for instance, windy situations (see Fig. 3). This force has been modelled trough a sine wave of frequency $\pi/4$ rad/s and 1 N amplitude. In order to model the wind effect blowing in only one direction, the force assumes zero values during the negative half-period of the wave. The

entire simulation time has a duration of 20 s, while the external force acts only for the first 10 seconds.

First, a rigid behavior has been imposed to the chosen Cartesian variables $\boldsymbol{x}$. The stiffness matrix in (22) has been tuned to $\boldsymbol{K}_p = 80\boldsymbol{I}_9$, while in order to choose $\boldsymbol{K}_D$, the values of the damping ratio for each component have been tuned to 0.8, so as not to have oscillations. The results of this simulation are shown in Fig. 4. In particular, Figs. 4(a)-4(c) show that, as desired, the vehicle and the manipulator end-effector do not move significantly from their initial conditions.

Then, a compliant behavior of the system is investigated. Now the stiffness matrix has been tuned to $\boldsymbol{K}_p = 5\boldsymbol{I}_9$, while the damping ratio values are 0.5 for each component. The results of this simulation are shown in Fig. 4. The compliant behavior is noticed looking at the increased values of the error norms in each time history of Figs. 4(d)-4(f). After that the effect of the external force is vanished, the system recovers the desired conditions.

In the case study B, an external force acts along the $\boldsymbol{x}_b$ axis of Σ_b with the same aforementioned modality. In addition, another force with 0.5 N of magnitude acts along the $\boldsymbol{a}_e$ end-effector axis for all the 20 s of simulation time. This scenario simulates, for instance, the case of the manipulator end-effector in contact with a wall, while the aerial manipulator should again deal with windy situations (see Fig. 3). Thereby, the manipulator end-effector position is chosen to be rigid, while the aerial vehicle pose is chosen to be compliant. Hence, the stiffness matrix in (22) has been tuned to $\boldsymbol{K}_p = \mathrm{diag}(10\boldsymbol{I}_6, 100\boldsymbol{I}_3)$, while the damping ratio values are 0.5 for the UAV components and 0.85 for the arm end-effector ones.

The results of this simulated case are shown in Fig. 4. The imposed high stiffness limits the oscillations of the position of the manipulator end-effector (see Fig. 4(g)). Since the contact force at the arm end-effector is always present, the Cartesian components error can be zeroed only along the unconstrained directions. On the other hand, the compliance behavior imposed to the position and orientation variables of the quadrotor can be observed in Fig. 4(h) and Fig. 4(i), respectively.

5. CONCLUSION AND FUTURE WORK

In this paper, the dynamic model of a UAV equipped with a robotic manipulator arm has been explicitly derived. A Cartesian impedance control has been employed in order to create a dynamic relationship between external generalized forces acting on the structure and the whole system motion. Two simulated case studies have been developed so as to test the proposed framework.

Future work will deal with exploiting the redundancy of the system, with respect to a given task, in order to accomplish some other subtasks, even in a prioritized order.

REFERENCES

Altug, E., Ostrowski, J., and Mahony, R. (2002). Control of a quadrotor helicopter using visual feedback. In *2002 IEEE International Conference on Robotics and Automation*, 72–77. Washington, DC.

Antonelli, G. (2006). *Underwater Robotics. Motion and Force Control of Vehicle-Manipulator Systems*, volume 2 of *Springer Tracts in Advanced Robotics*. Springer-Verlag, Berlin Heidelberg, D.

Bouabdallah, S. and Siegwart, R. (2007). Full control of a quadrotor. In *2007 IEEE/RSJ International Conference on Intelligent Robots and Systems*, 153–158. San Diego, CA.

Castillo, P., Lozano, R., and Dzul, A. (2005). Stabilization of a mini rotorcraft with four rotors. *IEEE Control Systems Magazine*, 25(6), 45–55.

Cheviron, T., Chriette, A., and Plestan, F. (2009). Generic nonlinear model of reduced scale UAVs. In *2009 IEEE International Conference on Robotics and Automation*, 3271–3276. Kobe, J.

Ghadiok, V., Goldin, J., and Ren, W. (2011). Autonomous indoor aerial gripping using a quadrotor. In *2011 IEEE/RSJ International Conference on Intelligent Robots and Systems*, 4645–4651. San Francisco, CA.

Grzonka, S., Grisetti, G., and Burgard, W. (2012). A fully autonomous indoor quadrotor. *IEEE Transactions on Robotics*, 28(1), 90–100.

Korpela, C., Danko, T., and Oh, P. (2012). MM-UAV: Mobile manipulating unmanned aerial vehicle. *Journal of Intelligent and Robotics Systems*, 65(1), 93–101.

Madani, T. and Benallegue, A. (2007). Sliding mode observer and backstepping control for a quadrotor unmanned aerial vehicles. In *Proceedings of the 2007 American Control Conference*, 5887–5892. New York City, NY.

Mahony, R. and Hamel, T. (2004). Robust trajectory tracking for a scale model autonomous helicopter. *International Journal of Robust and Nonlinear Control*, 14(12), 1035–1059.

Mahony, R., Stramigioli, S., and Trumpf, J. (2011). Vision based control of aerial robotic vehicles using the port Hamiltonian framework. In *50th IEEE Conference on Decision Control and European Control Conference*, 3526–3532. Orlando, FL.

Maza, I., Kondak, J., Bernard, M., and Ollero, A. (2010). Multi-UAV cooperation and control for load transportation and deployment. *Journal of Intelligent and Robotics Systems*, 57(1), 417–449.

Mellinger, D., Lindsey, Q., Shomin, M., and Kumar, V. (2011). Design, modelling, estimation and control for aerial grasping and manipulation. In *2011 IEEE/RSJ International Conference on Intelligent Robots and Systems*, 2668–2673. San Francisco, CA.

Michael, N., Fink, J., and Kumar, V. (2011). Cooperative manipulation and trasportation with aerial robots. In R. Tedrake and Y. Matsuoka (eds.), *Autonomous robots. Special issue: Robotics: Science and Systems*, volume 30, 73–86.

Nonami, K., Kendoul, F., Suzuki, S., Wang, W., and Nakazawa, D. (2010). *Autonomous Flying Robots. Unmanned Aerial Vehicles and Micro Aerial Vehicles*. Springer.

Ott, C. (2008). *Cartesian Impedance Control of Redundant and Flexible-Joint Robots*, volume 49 of *Springer Tracts in Advanced Robotics*. Springer-Verlag, Berlin Heidelberg, D.

Pounds, P., Bersak, D., and Dollar, A. (2011). Grasping from the air: Hovering capture and load stability. In *2011 IEEE International Conference on Robotics and Automation*, 2491–2498. Shanghai, CN.

Santibanez, V. and Kelly, R. (1997). Strict Lyapunov functions for control of robot manipulators. *Automatica*, 33(4), 675–682.

Siciliano, B., Sciavicco, L., Villani, L., and Oriolo, G. (2009). *Robotics. Modelling, planning and control*. Springer-Verlag, London, UK.

Siciliano, B. and Villani, L. (1999). *Robot Force Control*. Kluwer Academic Publishers.

Tayebi, A. and McGilvray, S. (2006). A fully autonomous indoor quadrotor. *IEEE Transactions on Control Systems Technology*, 14(3), 562–571.

Yamamoto, Y. and Yun, X. (1994). Coordinating locomotion and manipulation of a mobile manipulator. *IEEE Transactions on Automatic Control*, 39(6), 1326–1332.

Yoshida, K. and Wilcox, B. (2008). Space robots and systems. In B. Siciliano and O. Khatib (eds.), *Springer Handbook of Robotics*, 1031–1063. Springer.